Photon detection at subwavelength scales

Wang, Q.

Chapter 4

Optimal Design of NbN Superconducting Single-Photon Detectors

The microscopic detection mechanism in superconducting single-photon detectors causes the internal detection efficiency to depend on the position where the single photon is absorbed. This effect, together with the polarization-dependent optical absorption causes the detector response to be polarization dependent. We calculate the response of meandering wire NbN detectors by considering the optical response obtained from finite-different-time-domain simulations and the local detection efficiency measured by J. J. Renema et al. [Nano Lett. vol. 15, p. 4541, 2015] as input. The calculations show good agreement with experimentally measured polarization dependence in the internal detection efficiency of meandering wire detectors that were hitherto not understood. By considering the spatially non-uniform absorption in the wire we estimate an optimum wire width of 90 nm for detection of single photons at 1550 nm for light polarized with the E-field perpendicular to the wire[1].

4.1 Introduction

Superconducting single-photon detectors (SSPDs) [14] consist of a meandering nanowire made out of superconducting material through which a bias

[1] Q. Wang, et al. in preparation for publication.

current (I_b) is passed. Typically, this current is comparable in magnitude to the device critical current (I_c) below which the wire is superconducting. Absorption of a single photon of visible light is then sufficient to switch part of the wire from the superconducting to the normal state. This resistive state creates a voltage pulse that can be amplified and detected with pulse counting electronics. An appropriate design of the biasing electronics removes the current from the device in the normal state, allowing the detector to self-reset to the superconducting state on a nanosecond timescale [33].

The specific benefits of these detectors are their broad spectral range (from visible to infrared wavelengths) [18], combined with low dark-count rates [15], excellent timing resolution [16], and high detection efficiency [17]. This makes these detectors very suitable for use in quantum optics [76], quantum communication [77], and in the life sciences [63]. The optical response of these detectors under normal illumination is limited by the large impedance mismatch of the superconductor to vacuum or a dielectric [65]. For light incident from vacuum, this limits the maximum possible absorption efficiency to 50%. This limitation can be overcome by introducing a cavity structure that increases the absorption efficiency for wavelengths that are resonant to the cavity design [78], and device efficiencies up to 93% have been reported [17].

Recently, detector tomography on NbN *single nanowire* devices has been performed and has revealed a linear energy dependence of the detection probability [30]. This linear energy dependence can be explained by a microscopic detection model that uses quasiparticle diffusion and photon-assisted vortex entry [25, 30]. An important consequence of this microscopic detection model is that the photon detection efficiency depends on the position where the photon is absorbed because a photon absorbed in the middle of the wire affects the barrier for vortex entry to a much smaller extent than a photon absorbed at the edge of the wire. Using polarization resolved detector tomography [35] we were able to separate the effective absorption efficiency (η) of a nano-fabricated constriction from the internal detection efficiency (IDE). To capture the details of the microscopic detection mechanism a local detection efficiency ($LDE(x)$) that depends on the position x of photon absorption across the wire is introduced.

This $LDE(x)$ can be reconstructed from the measured IDE as a function of wavelength and polarization. To achieve this we use the numerically calculated position and polarization dependent absorption and an assumed linear exchange between current density and photon energy for each position across the wire [35]. This numerical inversion procedure leads to an estimate of the local detection efficiency that indeed predicts that photon absorption events occurring at the edge of a 150 nm wide wire are much more likely to produce a detection event than those in the middle. From these experiments we find that this "edge effect" extends roughly 30 nm into the wire, i.e., significantly

more than what was expected based on the theoretical predictions resulting from the microscopic model. An open question is whether, and to what extent the extracted spatially non-uniform $LDE(x)$ impacts the detection efficiency of *meandering* wire detectors.

To answer this question we compare the predictions based on the measured $LDE(x)$ to experimental data on the polarization-dependent absorption and detection efficiency of a set of meandering NbN SSPDs by Anant et al. [42]. These data show that the internal detection efficiency is less than 100% in state-of-the-art devices and depends on polarization. In this chapter we show how the $LDE(x)$ as determined in Chapter 3 can be used to quantitatively explain the measurements of Anant et al. Armed with a better understanding of the microscopic detection model we discuss the implications for the design of SSPDs to maximize photon detection efficiency for both polarizations. This design is a compromise between absorbing the photons at the edge of the wire where the $LDE(x)$ is maximum and optimizing the total absorption of the wire in a meander structure. We find that the optimal wire width for a NbN meandering SSPD operating at 1550 nm is $\sim$ 90 nm for polarization perpendicular to the wire, roughly three times the experimentally observed edge effect.

4.2 Photon detection process in NbN SSPDs

Absorption of a photon leads to the excitation of a single electron in the superconductor. For photon energies that are much higher than the superconducting gap this electron is strongly localized on a length scale well below the wavelength of the light. The energetic electron thermalizes via inelastic scattering with other electrons, Cooper pairs and the lattice, leading to a localized excitation of the superconductor [25]. [2]

Within the photon-assisted vortex-entry model, the thermalization process of the electron leads to a cloud of quasiparticles that diffuses in the superconductor and leads to a local decrease of the superconducting electron density (without creating a normal state). Because the potential barrier for vortex entry depends on the superconducting electron density, the probability for entry of a vortex from the edge of the wire is increased. Energy dissipation by

[2] We use photon-assisted vortex entry as the microscopic mechanism to explain a detection event. This choice is motivated by experimental observations that the current needed to get a 1% detection efficiency depends linearly on the total energy of the excitation [30]. The vortex is an essential ingredient to explain the experimental observation that the current extrapolated to zero photon energy does not correspond to the device critical current [25,30]. Photon-assisted vortex entry predicts that detection of a zero energy photon occurs at ~ 0.8 times the depairing current of the superconductor and also explains the observed temperature dependence [30].

the moving vortex breaks the superconducting state and triggers a photon detection event. An absorption event at the edge lowers the superconducting electron density at the edge of the wire and diverts supercurrent towards the center of the detector. Photon absorption in the center of the wire has little influence on the superconducting electron density at the edge of the wire, but diverts supercurrent towards the edge of the wire. For a NbN wire the lowering of the superconducting electron density at the edge is the dominant contribution to the decrease of potential barrier for vortex entry, therefore photon detection at the edge of the wire is more efficient than in the center. It thus becomes necessary to introduce a local detection efficiency $LDE(x)$ as a function of position x across the wire.

It is well-known that the response of an SSPD depends on photon energy and device bias current. For a constant photon energy, the response increases exponentially as a function of bias current and saturates above a threshold current. Following Ref. [35] we posit a relation between the local detection efficiency $LDE(x)$, bias current I_b and threshold current $I_{th}(x)$, where the position dependence is expressed through the position dependence of the threshold current:

$$LDE(x, I_b) = \min\{1, \exp[(I_b - I_{th}(x))/I^*]\}, \tag{4.1}$$

where I^* is a current scale that can be extracted from experiments by fitting the internal detection efficiency IDE as a function of I_b. In this chapter we use a value of $I^* = 0.65$ μA based on the experimental data in Ref. [35]. $LDE(x)$ changes with different parameters of I_b is well described by Eq. (4.1). We limit the discussion to single-photon detection at a constant wavelength of 1550 nm, allowing us to ignore the fact that the threshold current depends on photon energy.

The empirical model discussed above is sufficient to describe measured results on a NbN single wire SSPD [35], as well as numerical calculations of the detection process based on the photon-assisted vortex-entry model. The $LDE(x)$ derived from experiments indicates that the detection efficiency is roughly constant for distances up to ~ 30 nm from the edge of the wire, while numerical results indicate a much more rapid decrease in the detection efficiency. Currently, the difference between these two curves is not understood. Throughout this chapter we use the experimentally determined values because we intend to discuss the implications of $LDE(x)$ on the performance of meandering detectors and future detector design.

4.3 Optical absorption and detector response

To calculate the response of a meandering SSPD both the local detection efficiency $LDE(x)$ and the spatial distribution of optical absorption $A(x)$ need to be taken into account. The $LDE(x)$ determines the probability to generate a click once a photon is absorbed at position x and contains the detailed physics of the microscopic detection model. The factor $A(x)$ determines the macroscopic probability to absorb the photon at position x and can be calculated to good accuracy using standard numerical procedures to solve Maxwell's equations. We use finite-difference-time-domain (FDTD, FullWave package, RSoft [71]) simulations in two dimensions by approximating a meandering SSPD by an infinitely large array of wires via imposing periodic boundary conditions. We ignore bends in the meandering wire and limit ourselves to a plane wave incident at normal incidence. The first approximation is justified because in an actual SSPD the area covered by straight wire is much larger than the area of the bends. In addition, the central part of the meander is illuminated by making the light spot (diameter of ~ 10 μm) slightly smaller than the meander size. The assumption that the optical absorption of a meandering detector is well described by plane-wave illumination at normal incidence relies on the fact that the illuminating beam has a small numerical aperture (~ 0.1) and that the absorption is to first order independent of angle of incidence near normal incidence [65].

Figure 4.1(a) shows the cross section (not to scale) of a repeat unit (width p) of the periodic structures used in the FDTD calculation. A 4.35 nm thick NbN nanowire (width w) with a 2 nm thick oxide layer of NbN_xO_y lies on top of a semi-infinite sapphire substrate. The fill factor f of the wires in a meandering wire is defined as w/p. The refractive indices of all the materials are taken from Ref. [42]: $n_{sapphire} = 1.75$, $n_{NbN} = 5.23 + 5.82i$, and $n_{_{NbNO}} = 2.28$. In the calculation, a plane wave, at wavelength of 1550 nm, illuminates the structure from the top (y-direction) and has the electric field either parallel ($\parallel$) or perpendicular ($\perp$) to the wire. The simulation area is bound by a perfectly matched layers (PML) on top and beneath the structure. The boundary conditions on the left and right boundary (see B.C. in Fig. 4.1(a)) can be set to PML to calculate the properties of an isolated wire or to periodic boundary condition to calculate the properties of a meandering structure.

The ~ 4 nm thick NbN film is much thinner than the skin depth of ~ 90 nm at the relevant wavelength of 1550 nm. Hence, the absorption distribution is uniform over the thickness of the film and is a function of position x across the nanowire only and can be expressed as follows [79]

$$A(x) = \frac{P_{abs}(x)}{P_{total}/w} = \frac{\int_0^t \frac{1}{2}\omega\varepsilon_o \mathrm{Im}(\varepsilon_{_{NbN}})|E(x,y)^2|dy}{P_{total}/w}, \tag{4.2}$$

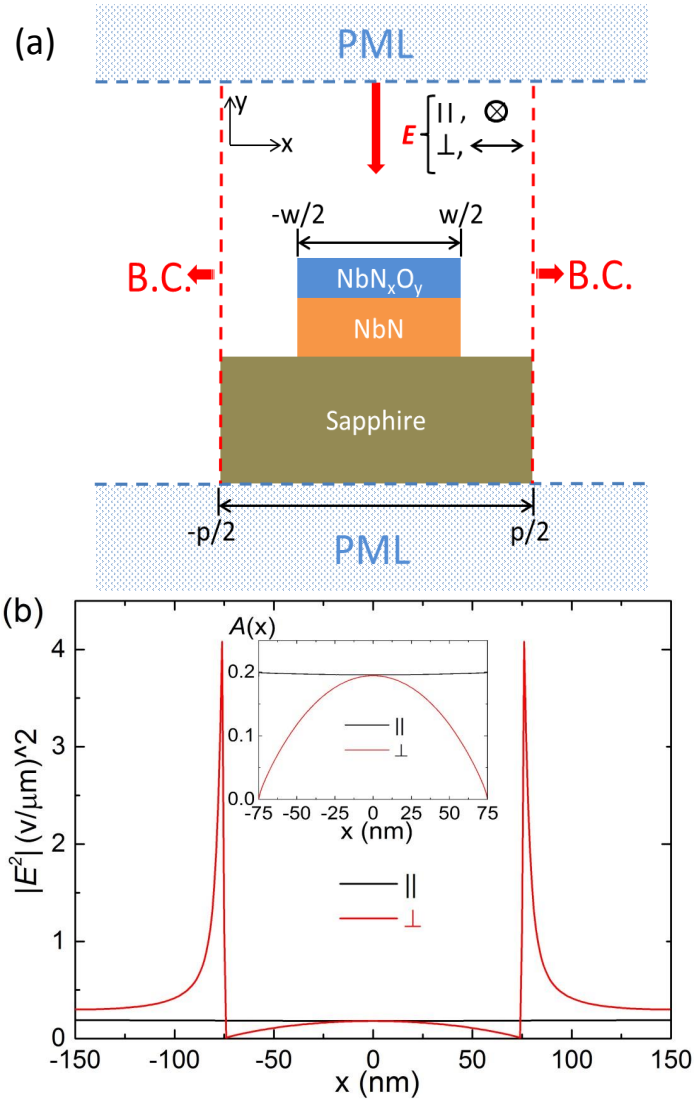

Figure 4.1: (a) Cross section of a simulation cell in the 2D FDTD calculation. The boundary conditions at $x = \pm\, p/2$ are adapted to simulate either a periodic array of wires or an isolated wire. Inside the computational cell the 4.35 nm thick NbN wire ($n_{_{NbN}} = 5.23 + 5.82i$) with width w is sandwiched between a semi-infinite sapphire substrate ($n_{_{sapphire}} = 1.75$) and a 2 nm thick oxidation layer NbN_xO_y ($n_{_{NbNO}} = 2.28$). A linearly polarized plane wave with a wavelength of 1550 nm and E-field either parallel ($\|$) or perpendicular ($\perp$) to the wire is incident from the top of the structure. (b) Calculated intensity distribution $|E^2|(x)$ for a periodic array of 150 nm wide wires with a pitch $p = 300$ nm. The field distribution for parallel polarization is almost uniform, while the distribution for perpendicular polarization shows two strong discontinuities caused by singularities occurring at the edges of the NbN wire. The inset shows the absorption distribution inside the NbN wire in more detail.

where w is the width of the wire, P_{total}/w is the power density of illumination across the wire, $P_{abs}(x)$ is the absorbed power density as a function of position x across the wire width, ω is the angular frequency of the incident light, ε_o is the vacuum permittivity, $t = 4.35$ nm is the thickness of the NbN film, and $|E(x,y)^2|$ is the electric field intensity in the wire.

As an example, Fig. 4.1(b) shows the time averaged $|E(x)^2|$ across a $w = 150$ nm wide wire in a meander with a $p = 300$ nm wide pitch. For illumination with parallel polarization, $|E(x)^2|$ is almost constant over the entire unit cell. For perpendicular polarization, singularities in the field appear at the edge of the wire ($x = \pm$ 75 nm). The singularities originate from the electric field distribution around the sharp right-angle wedges of the wire. The inset shows the optical absorption distribution $A(x)$ inside the wire in more detail. It is important to note that the highly non-uniform spatial distribution of the absorption in case of perpendicular polarization is related to the edges of the wire, and that the calculated profile $A(x)$ for periodic structures is very similar to a calculation for a single wire [35] provided that the pitch of the meander is smaller than the wavelength.

We obtain the $LDE(x)$ from Eq. (4.1) using the experimentally determined value of $I_{th}(x)$ for photons with a wavelength of 1550 nm (0.8 eV energy) [35]. Figure 4.2(a) shows the results of the $LDE(x)$ at bias currents $I_b = 0.8I_c$, $0.9I_c$ and I_c. As can be seen in the figure, the edges of the wire have much higher local detection efficiency than that of the center for sufficiently low bias currents. As the bias current increases, the detection efficiency at the edge starts to saturate. For currents close to the critical current $LDE(x)$ becomes equal to unity over the entire width of the wire. It is important to note that the values of the critical currents and threshold currents used to define $LDE(x)$ refer to those of a nanodetector (see Chapter 3). For longer wires, inhomogeneities and other imperfections in the wire directly limit the device critical current. The threshold current is affected in a different way because the sections of wire that are not biased close to their critical current will still detect photons. As a result the ratio between the device critical current and the threshold current for a meandering wire is expected to be closer to one than the same ratio for a nanodetector.

Similar to the short wire calculation, we assume that the overall detection probability or the response of a meandering SSPD can be expressed by:

$$R(I_b) = \frac{\int_{-w/2}^{w/2} A(x) \cdot LDE(x, I_b) \mathrm{d}x}{w} \tag{4.3}$$

where w is the width of the wire.

Figure 4.2(b) shows the response distribution $r(x) = A(x) \cdot LDE(x, I_b)$ for both polarizations. The solid and dashed curves correspond to parallel and

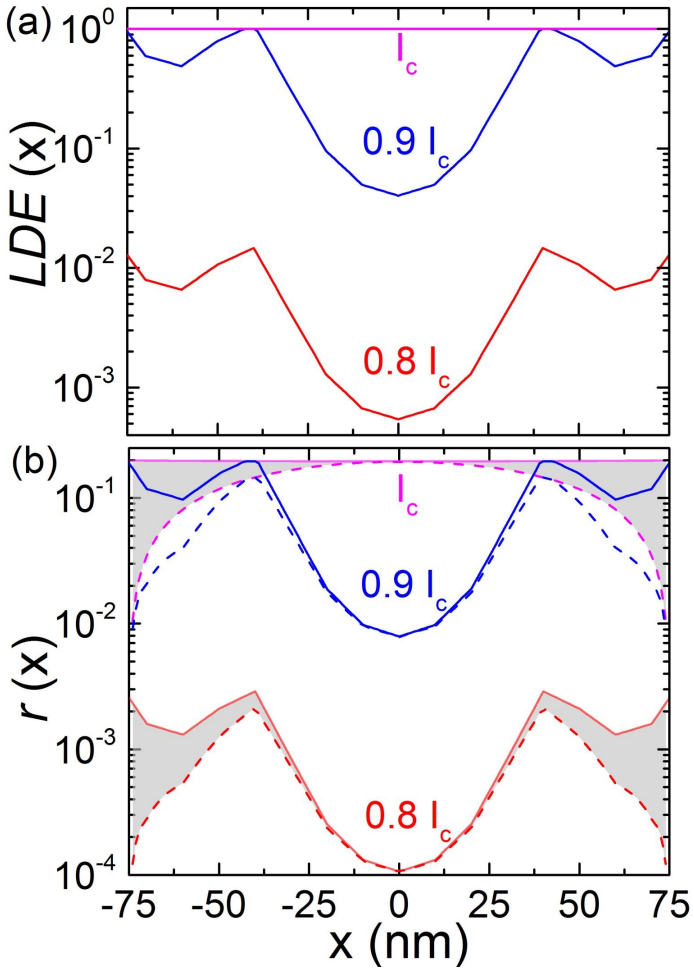

Figure 4.2: (a) Local detection efficiency across the 150 nm wide NbN wire at values of the bias current equal to $0.8I_C$, $0.9I_C$ and I_C. The curves are determined experimentally in Ref. [35]. (b) Detection response distribution across the 150 nm wide NbN wire at the same bias currents as shown in (a). The solid and dashed curves represent parallel ($\parallel$) and perpendicular ($\perp$) polarization, respectively. The grey area between the solid and dashed curves at bias currents of $0.8I_C$ and I_C shows the difference of the local response between the two polarizations. For reasons of clarity the area between the two curves at $0.9I_C$ is not filled. The curves at $0.9I_C$ are used to produce the results in the remaining of this chapter.

perpendicular polarization, respectively. The calculated response distribution is plotted for various values of the bias currents (I_b = 0.8 I_c, 0.9 I_c and I_c). For the highest bias current, i.e., $I_b = I_c$, the $LDE(x)$ equals to one over the wire, and the response distribution $r(x)$ reflects the profile of the absorption distribution $A(x)$, which is shown in the inset of Fig. 4.1(b). The areas between the solid and dashed curve for each bias current (e.g., filled with grey for $0.8I_c$ and I_c) illustrate the difference in local response between the two polarizations. The detector response $R(x, I_b)$ is then calculated by the integral of the local response $r(x)$ as given by Eq. (4.3). In the following sections we use the $LDE(x)$ at a bias current of $0.9I_c$ to calculate the detector response for other geometries of meandering SSPDs, because this value of bias current gives the best agreement with the data presented in Ref. [42].

4.4 Results

4.4.1 Detector response for SSPDs with a constant wire width

Figure 4.3 shows the calculated detector response R as a function of the average optical absorption for a set of meander structures with a constant wire width w and different values of the pitch p = 150 nm, 200 nm, 300 nm, 400 nm and 500 nm. The average optical absorption is straightforwardly calculated by averaging the absorption distribution:

$$\bar{A} = \frac{1}{w}\int_{-w/2}^{w/2} A(x)\mathrm{d}x.$$

The solid, diagonal line with slope one indicates a detector with 100% internal detection efficiency for which each absorbed photon triggers the detector. Calculated data points for meander structures illuminated with parallel polarization (solid circles) and perpendicular (open circles) are shown and are fitted to a linear dependence. The fact that the detector response is proportional to the average absorption implies that meandering wires of constant width but different pitches have the same internal detection efficiency of the wire. For a constant wire width, the absorption distribution $A(x)$ resembles that of an isolated wire and is very similar for structures with different pitches.

For both polarizations, the average absorption $\bar{A}$ is mainly determined by the fill factor f, which is given by the ratio of wire width w over the pitch p, and increases as f increases (i.e., for decreasing p), as expected [65]. Typically the IDE of the SSPDs (slope of the dashed line) with parallel polarization is higher than that of SSPDs with perpendicular polarization. This can be explained by the different $A(x)$ for the two polarizations as shown in the inset of Fig. 4.3. As an example, for structure of w = 100 nm and p = 300 nm, the

$A(x)$ in parallel polarization is spatially uniform and higher than the calculated $A(x)$ for perpendicular polarization.

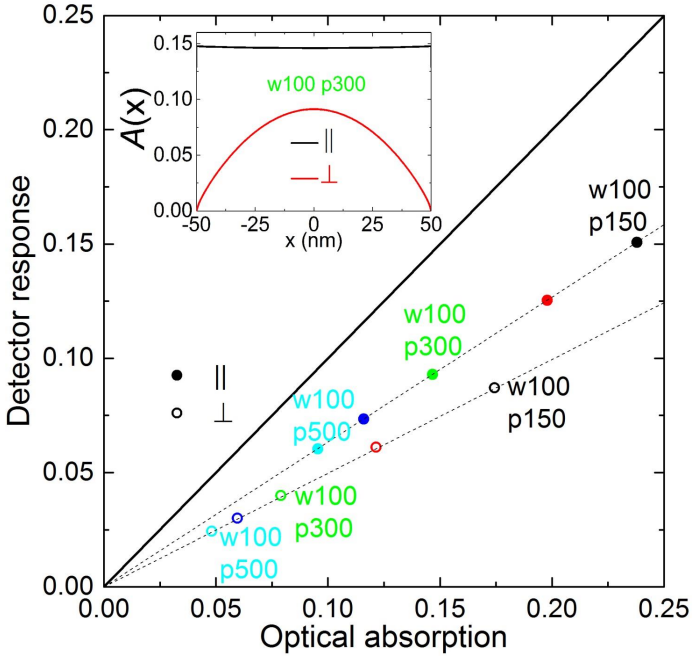

Figure 4.3: Calculated detector response as a function of optical absorption of meandering SSPDs with constant wire width ($w = 100$ nm). The closed and open symbols represent parallel ($\|$) and perpendicular ($\perp$) polarization, respectively. The numbers next to the data points refer to the constant width w and varying pitch p expressed in nm. The inset shows a typical absorption distribution across the wire for structure with $w = 100$ nm and $p = 300$ nm. The diagonal line with slope of 1 represents IDE with a value of 1.

4.4.2 Detector response for SSPDs with constant fill factors

Figure 4.4 shows the calculated response of meandering SSPDs with constant fill factors as a function of the average absorption for both polarizations. The solid and open symbols represent polarization states with the E-field parallel and perpendicular to the wire, respectively. For comparison, the triangles and squares represent structures with fill factor of $f = 1/2$ and $f = 2/3$. The wire width w is set from 50 nm to 150 nm with a step of 10 nm, except for the structures with $f = 1/\ 2$ in perpendicular illumination, where extra settings of w of 5 nm, 10 nm, 20 nm, 30 nm, 40 nm, 50 nm are considered (open triangles) as well.

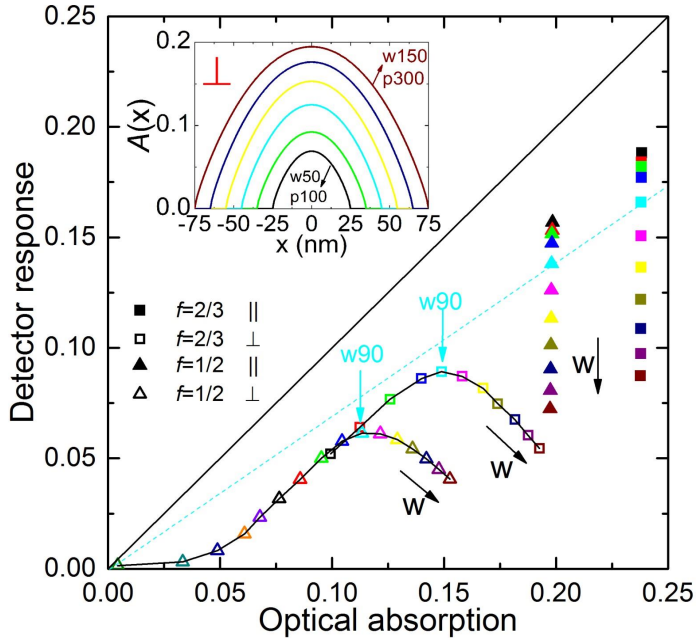

Figure 4.4: Calculated detector response as a function of optical absorption of SSPD meandering structures with varying wire width and constant fill factor of 1/2 (triangles) and 2/3 (squares). The closed and open symbols refer to parallel (||) and perpendicular (⊥) polarized light, respectively. The arrow indicates increasing width of the wire. The inset shows the absorption distribution for perpendicular polarized light as a function of wire width (fill factor 1/2). The diagonal line with slope of 1 represents IDE with a value of 1.

For parallel polarization (solid symbols), the absorption distribution across the wire is almost uniform and the average absorption $\bar{A}$ is mainly determined by the constant value of f; the data points lie on a vertical line in the figure. The difference between the points is caused by a change in the internal detection efficiency as a function of wire width w. When comparing the two different fill factors, the structures with a constant wire width w (e.g., w= 90 nm in light blue) lie on a straight line through the origin (see the dashed line) as shown in Fig. 4.3, which represents a constant internal detection efficiency of the wire.

The data for perpendicularly polarized light for a constant fill fraction f and increasing w (direction of the arrow in Fig. 4.4) show a maximum in response R for a wire width around $w = 90$ nm, for both values of the fill factor. The internal detection efficiency IDE increases sharply with wire width for very narrow wire and decreases with the width as w increases beyond $w = 90$ nm. This behavior originates from the dependence of the $LDE(x)$ as a function of wire width in combination with the non-uniform absorption distribution for perpendicularly polarized light. To obtain the $LDE(x)$ for wires that are narrower than 150 nm we use the result of Fig. 4.2(a) for a 150 nm wide nanowire and omit the central part of the curve, leaving only the highly efficient edges of the wire. This procedure is motivated by numerical calculations of the $LDE(x)$ [25] that show that removing the central part of the curve of a wide wire correctly predicts the behavior of narrower wires.

Experiments show a linear exchange between input photon energy E and bias current: $I_b = I_o - \gamma E$, where γ represents the interchange ratio between bias current and photon energy and I_o is a reference current beyond which the vortices enter the nanowire [30, 38]. In the photon detection model, a microscopic relation between $I_{th}(x)$ and photon energy is assumed as $I_{th}(x) = I_c - \gamma'(x) * E$, where $\gamma'(x)$ is the position-dependent interchange ratio between threshold current and photon energy. We note that the calculated average $\overline{\gamma'(x)}$ from the model does not agree with the value of γ reported for three SSPDs with different widths [30]. The origin of this discrepancy is currently unclear, but may be caused by statistical fluctuations given the limited amount of experimental data. Making $\gamma'(x)$ consistent with the measured γ leads to a change in the response shifting the curves in Fig. 4.4 up, leaving the optimum wire width unaffected to first order.

Because the edge has a higher detection efficiency than the center, the narrower wire has a higher average $LDE(x)$ and a higher IDE and thus R for parallel polarization. With perpendicular illumination the absorption distribution as a function of wire width is an important factor. As the wire width rises, the average of $LDE(x)$ decreases, but is compensated by an increase of the average absorption $\bar{A}$, as shown in the inset of Fig. 4.4. Because the $LDE(x)$ is approximately constant for the first $\sim$ 30 nm from the edges and the average absorption increases with the wire width, the response of the de-

tector increases as a function of wire width until $w \sim 60$ nm. For a wire width beyond ~ 60 nm, there is a trade-off for the wire to be narrow enough to have a high $LDE(x)$ and to be wide enough to have high optical absorption $A(x)$. This trade-off depends on the detailed shape of the absorption, the bias current relative to the threshold current and the wavelength of the light used. For the parameters considered in this chapter the trade-off results in an optimal value of $w \approx 90$ nm, almost three times the width of the side-wing in the $LDE(x)$ profile.

4.4.3 Comparison between calculation and experiment

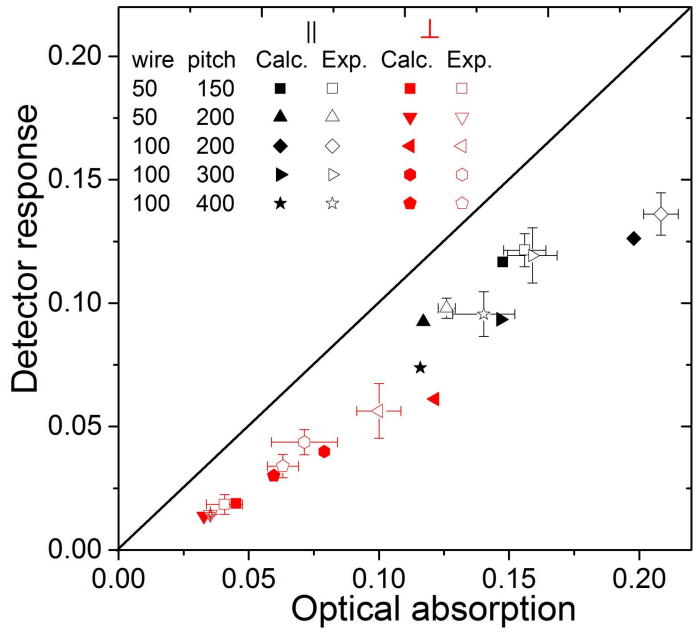

Figure 4.5: Measurements [42] and calculations of detector response as a function of optical absorption of meandering SSPDs. The open symbols represent experimental data as presented in Ref. [42]. The closed symbols refer to the calculated response based on the local detection efficiency $LDE(x)$ for $I_b = 0.9I_C$. Black and red symbols represent parallel ($\parallel$) and perpendicular ($\perp$) polarization, respectively. Different symbol shapes refer to different structures (wire and pitch width) of the detector. The error bars on the experimental data represent the spread in properties between detectors of the same design. The diagonal line with slope of 1 represents IDE with a value of 1.

In order to verify our photon-detection model and optical absorption simulation, we calculate and compare the detector response for the structures used

in the experiment of Ref. [42]. Figure 4.5 shows the comparison of our calculation (solid symbols) with the experimental data (open symbols). Symbols in black and red represent parallel and perpendicular polarization, respectively. Good agreement between calculation and experiment is shown. The calculation confirms the hypothesis in Ref. [42] that the data with parallel polarization has a larger IDE (slope) than those for perpendicular polarization. We stress that the layout of the data points for calculation and experiment are strongly correlated, e.g., the rhombuses for calculations and measurements for a structure of $w = 100$ nm and $p = 200$ nm are located in the top right corner of data cluster for both polarizations. The use of the local detection efficiency $LDE(x)$ that is supported by a microscopic detection model of photon-assisted vortex entry explains why the IDE depends on the detector geometry. The experimentally determined $LDE(x)$ gives a quantitative description of the effect.

To obtain a non-unity IDE, we must assume that the highly efficient detectors reported in Ref. [42] were not biased to the depairing current of NbN. This assumption is quite reasonable because it is well known that the presence of inhomogeneities and current crowding in the bends of a wire can cause a reduction of the device critical current relative to the maximum possible depairing current. Such effects are expected to be much more prominent in long meandering wires as compared to a nanodetector. Current crowding in bends can reduce the critical current by as much as 40%, with typical values of 10–20% [26]. To get good agreement between experimental data and the calculation we have assumed $I_b = 0.9\ I_c$ for all devices to produce Fig. 4.5. This demonstrates that our calculations quantitatively describe the SSPDs which are used for applications, at the typical currents at which they are operated.

The agreement between calculation based on the detection model and the experimental data justifies the procedure to obtain the $LDE(x)$ for wire widths smaller than 150 nm.

4.5 Conclusions

We have calculated the optical absorption and E-field distribution of meandering SSPDs via FDTD simulation. The absorption distribution is uniform across the nanowire when illuminated with E-field parallel to the wire. For perpendicularly polarized light the absorption close to the edges is minimal while the center of the wire displays maximum absorption. The response of an SSPD can be calculated by taking into account a local detection efficiency obtained from experiment and the absorption distribution. We have used this procedure to calculate the detector response for meandering SSPDs with different pitch and wire widths. For SSPDs with a constant wire width, the internal detection efficiency is predominately determined by the wire width, and higher fill

factor leads to higher detector response. For SSPDs with a constant fill factor, the detector response curve for perpendicular polarization shows an optimal design for $w = 90$ nm that represents a trade-off between the wire being wide enough to efficiently absorb the incoming light while still being narrow enough to have a high local detection efficiency. To validate our calculations and the use of the experimentally determined local detection efficiency from Renema et al. (Ref. [35]) we compare the predictions with experimentally observed values from Anant et al. (Ref. [42]). The good quantitative agreement confirms that the local detection efficiency obtained for a nanodetector can be used to make quantitative predictions for state-of-the-art meandering wire detectors. More importantly, it shows how the idea of a photon-assisted vortex-entry model that results in a position-dependent local detection efficiency quantitatively explains a polarization-dependent internal detection efficiency.